Synchronous Northern and Southern Hemisphere response of the westerly wind belt to solar forcing

Supporting Information

This section contains supporting information and figures referred to in the main text.

Study site – climate

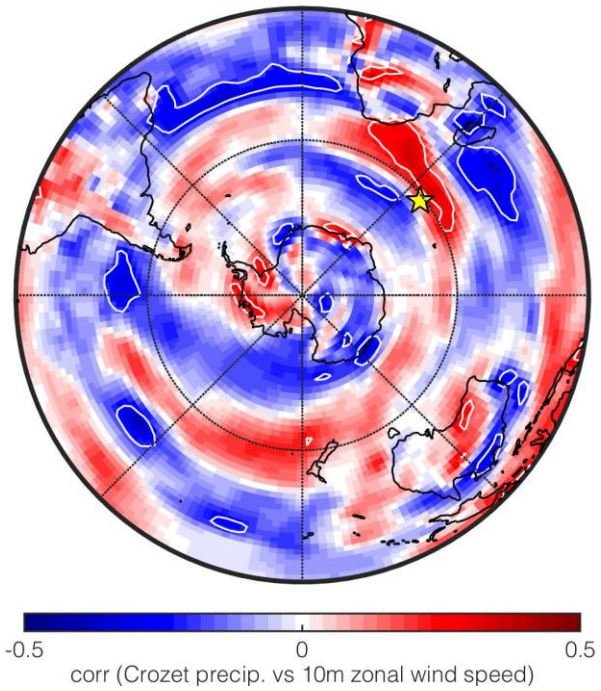

Figure S1: Correlation of December to February (DJF) precipitation at Crozet (yellow star) to 10m zonal wind speed in the southern hemisphere between 1960 and 2010 C.E. Areas where wind speed is significantly (90%) correlated to Crozet precipitation, are encompassed by white contour lines. The precipitation is extracted as the latitudinally weighted mean precipitation in a box from 49 – 44^{0}S and 50 – 55^{0}E from the 20th century reanalysis V2c (Compo et al., 2011) and correlated to the 10m zonal wind speed at every other grid cell from the same reanalysis data set. It can be seen that DJF precipitation at Crozet correlates positively with wind zonal speeds just north of the Island.

Chronology

Morne Rouge peat sequence

The previous chronology of the Morne Rouge sequence was based on five ^{14}C (Van der Putten et al., 2008). To establish a high-resolution chronology, focused on the period around 2800 cal yr BP, we additionally ^{14}C dated 17 new macrofossil samples (Supplementary Table S1). We applied ^{14}C wiggle-match dating (Pearson, 1986; van Geel and Mook, 1989) to build the age-model. The samples were thus selected to match the distinct structure of the ^{14}C calibration curve around the period 3000-2000 cal yr BP, which shows two rapid increases in the atmospheric ^{14}C concentration (rapid ^{14}C age decreases) with decreasing atmospheric ^{14}C values in between (leading to a so-called ^{14}C-age-plateau) (Reimer et al., 2013). Wiggle-match dating has previously been applied to peat sequences to constrain time-scales (Mauquoy et al., 2002; Mellström et al., 2015). The samples underwent pre-treatment with NaOH and HCl prior to graphitisation and they were measured at the Single Stage AMS facility at Lund University(35, 36). The ^{14}C age-model was constructed using OxCal version 4.2 (Bronk Ramsey, 2009) with the implemented P_Sequence deposition model (Bronk Ramsey, 2008) and the SHCal13 Southern Hemisphere ^{14}C calibration curve (Hogg et al., 2013). The difference between the SHCal13 and SHCal20 calibration curve is negligible for the Holocene in general (especially when considering the 2σ range) and around the period of interest in particular (Hogg et al, 2020).

All 22 ^{14}C dates shown in Supplementary Table S1 were added to the age-model, however, three of them were considered as outliers. Two of these samples (LuS-9753 and LuS-10081) were rejected since they obviously had non-consistent ^{14}C dates. Two samples (LuS-9754 and LuS-9755) were dated at the same depth of 251 cm. However, based on a poor fit with a very low agreement index (see Bronk Ramsey, 2009), the sample LuS-9755 was considered as an outlier. Different step-wise values to account for peat accumulation rate variations ("k-values" see Ref. Bronk Ramsey, 2008) were applied to the age-model. The model becomes more (less) rigid with increasing (decreasing) k-values. This means that with a low k-value, the age model would be similar to a Sequence (only knowing the order of the dated events) and with a high k-value the model would become similar to the U_Sequence (uniform/constant deposition rate). To statistically determine the most accurate age model, the agreement index was used. We performed a step-by-step approach, starting with a low k-value and increasing it by steps of 0.1. Already at a k-value of 0.1 there were two samples with agreement indices below 60%, however, the samples were included in the age models. At k-values higher than 0.7 there were additional samples with individual agreement indices below 60%. This means that the age model had become too rigid. The k-value was therefore set to 0.7 for the final age model based on the agreement index. None of the rejected ^{14}C measurements was close to the climate transition that we discussed in this study.

To test the robustness of our age model we did runs with different k-values. We do not get significantly different results depending on what age model (k-value) we use for the timing of the transition we are interested in. Below we show the age range 2σ (1σ) and median for different k-values applied for the Sample LuS-10085 (depth 294 cm, around the timing of the transition):

The final age model used in our study with a k-value 0.7, Table S1: 2771-2692 (2751-2716), median 2733.

The age model with a k-value 1: 2778-2700 (2755-2720), median 2738.

The age model with a k-value 0.1: 2765-2620 (2750-2704), median 2724.

This shows that our age model is very robust around the period of interest.

The wiggle-matched age-model for the period around 2800 cal yr BP is shown in Fig. S2. The age-depth model for the complete Morne Rouge sequence is shown in Fig. S3 (see also Table S1). The mean age uncertainty for all samples is ca. ±65 years (95.4% probability range). For the period from 2800 to 2500 cal yr BP the mean age uncertainties are ca. ±55 years (95.4% probability range). The smallest age uncertainties (ca. ±40 years, 95.4% probability range) are obtained for the samples dated to the two periods of rapid increases of atmospheric ^{14}C concentration.

Table S1: ^{14}C data for the Morne Rouge peat record. Included are five dates previously published by Van der Putten et al. (2008) and three outliers[x].

Lab-no	Depth (cm)	^{14}C BP	Modelled age cal yr BP 95.4% probability (68.2%)	Median age cal yr BP
KIA-32605[*]	64.5	720±25	661-560 (593-567)	582
KIA-32602[*]	169.5	1510±25	1414-1315 (1406-1338)	1364
LuS-9753[x]	246	980±45	-	-
LuS-9755[x]	251	2040±45	-	-
LuS-9754	251	2270±45	2285-2160 (2262-2198)	2228
LuS-10078	254	2240±40	2310-2198 (2290-2234)	2260
LuS-10080	258	2225±40	2340-2257 (2323-2284)	2301
LuS-9756	260	2375±45	2379-2299 (2353-2317)	2336
LuS-10081[x]	264	2095±40	-	-
LuS-9758	272	2540±45	2568-2420 (2530-2460)	2496
KIA-32604[*]	279.5	2650±25	2638-2515 (2631-2545)	2577
LuS-10082	280	2390±45	2650-2525 (2639-2550)	2587
LuS-9759	284	2450±45	2680-2576 (2665-2596)	2640
LuS-10083	285	2435±45	2686-2590 (2673-2602)	2648
LuS-10084	289	2450±45	2716-2635 (2700-2660)	2678
LuS-10085	294	2605±50	2771-2692 (2751-2716)	2733
LuS-10086	298	2655±45	2855-2737 (2845-2746)	2787
LuS-10390	302.5	2984±35	3104-2893 (3041-2960)	3005
LuS-10391	310.5	3081±40	3253-3074 (3222-3083)	3174
LuS-10392	319.5	3158±45	3395-3210 (3361-3247)	3292
KIA-32603[*]	405.5	4050±30	4567-4413 (4514-4429)	4475
NZA-11509[*]	532.5	5480±60	6305-5995 (6285-6020)	6185

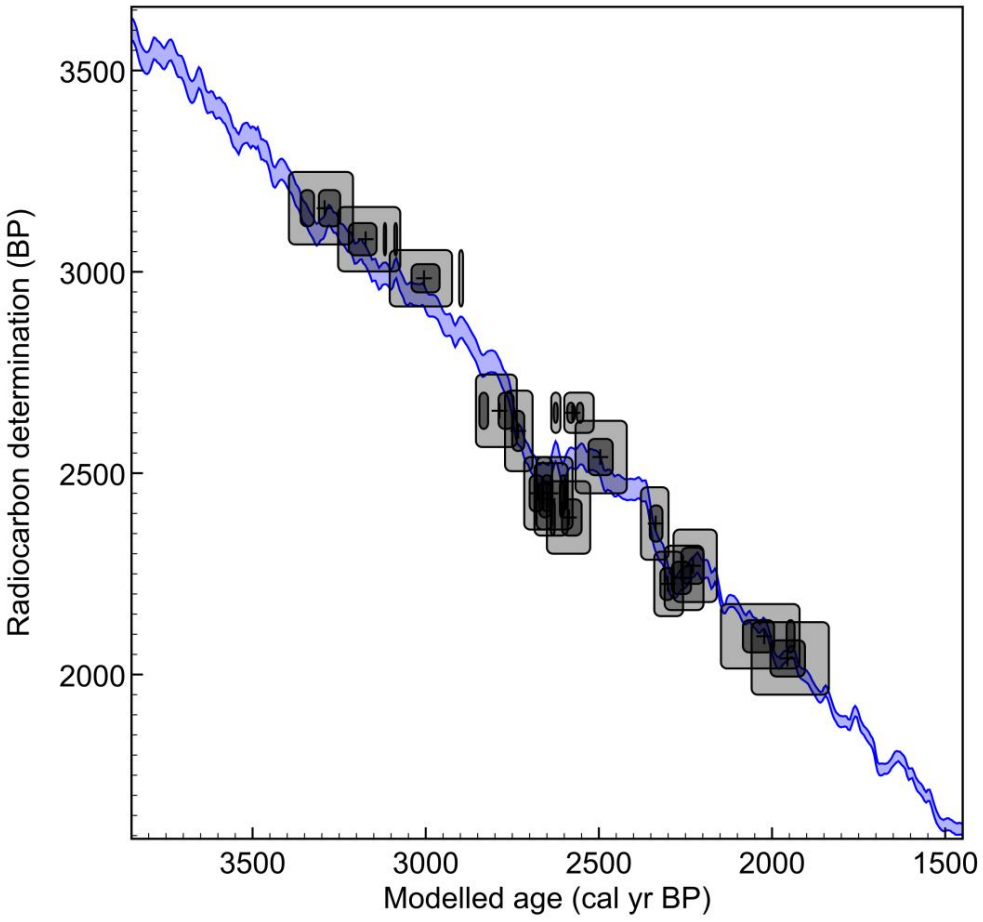

Figure S2: Age-model for the peat sequence sequence focused on the period around 2800 cal yr BP. The modelled ages are shown with the 95.4% and 68.2% probability ranges (lighter respectively darker grey areas) and the median ages are indicated by the symbols. The SHCal13 ^{14}C calibration curve (Hogg et al., 2013) is shown in blue.

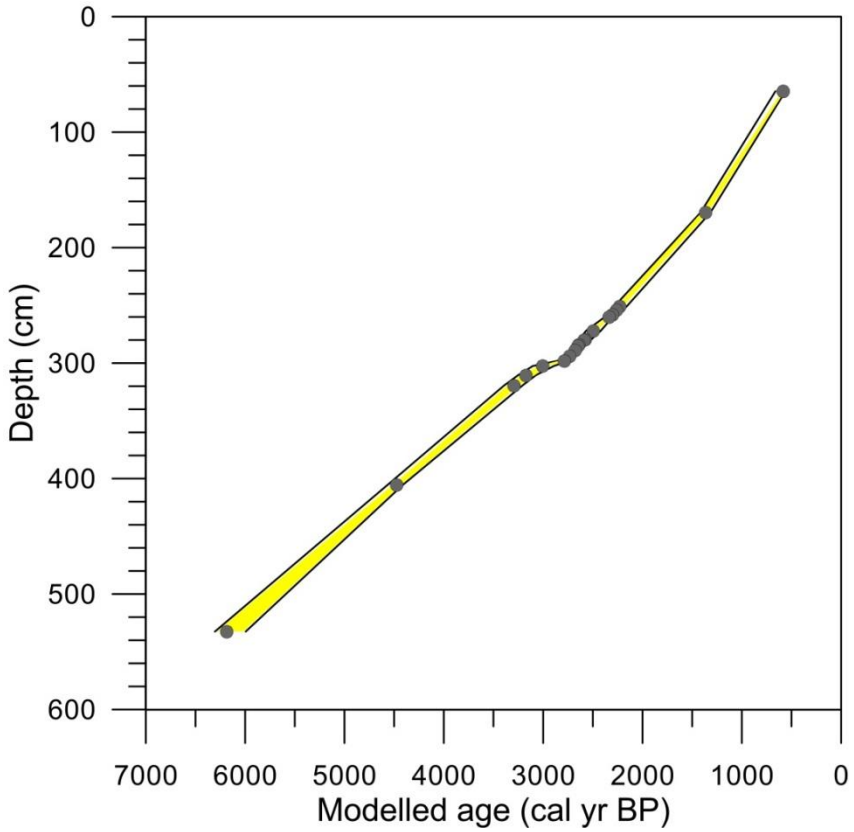

Figure S3: Age-depth model for the complete peat sequence sequence based on the ^{14}C wiggle-match dating results presented in Table S1 and shown in Fig. S2. The median ages are indicated by grey dots. The solid black lines and yellow coloured area indicate the 95.4% and 68.2% probability ranges, respectively.

Morne Rouge lake sequence

Four macrofossil samples were ^{14}C dated as described above. Calibration of the single dates was done in OxCal version 4.2[10] using the SHCal13 Southern Hemisphere ^{14}C calibration curve (Hogg et al., 2013)

Table S2: ^{14}C data for the Morne Rouge lake record.

Lab-no	Depth (cm)	^{14}C BP	Age cal yr BP 95.4% probability (68.2%)	Median age cal yr BP
LuS-10766	25.5	2098±70	2302-1840 (2144-1929)	2033
LuS-10767	38.5	2318±35	2354-2160 (2348-2189)	2301
LuS-10768	56.5	2581±35	2751-2489 (2744-2507)	2618
LuS-10769	68.5	2665±35	2848-2546 (2776-2735)	2753

Study site – Ile de la Possession and location of Morne Rouge volcano

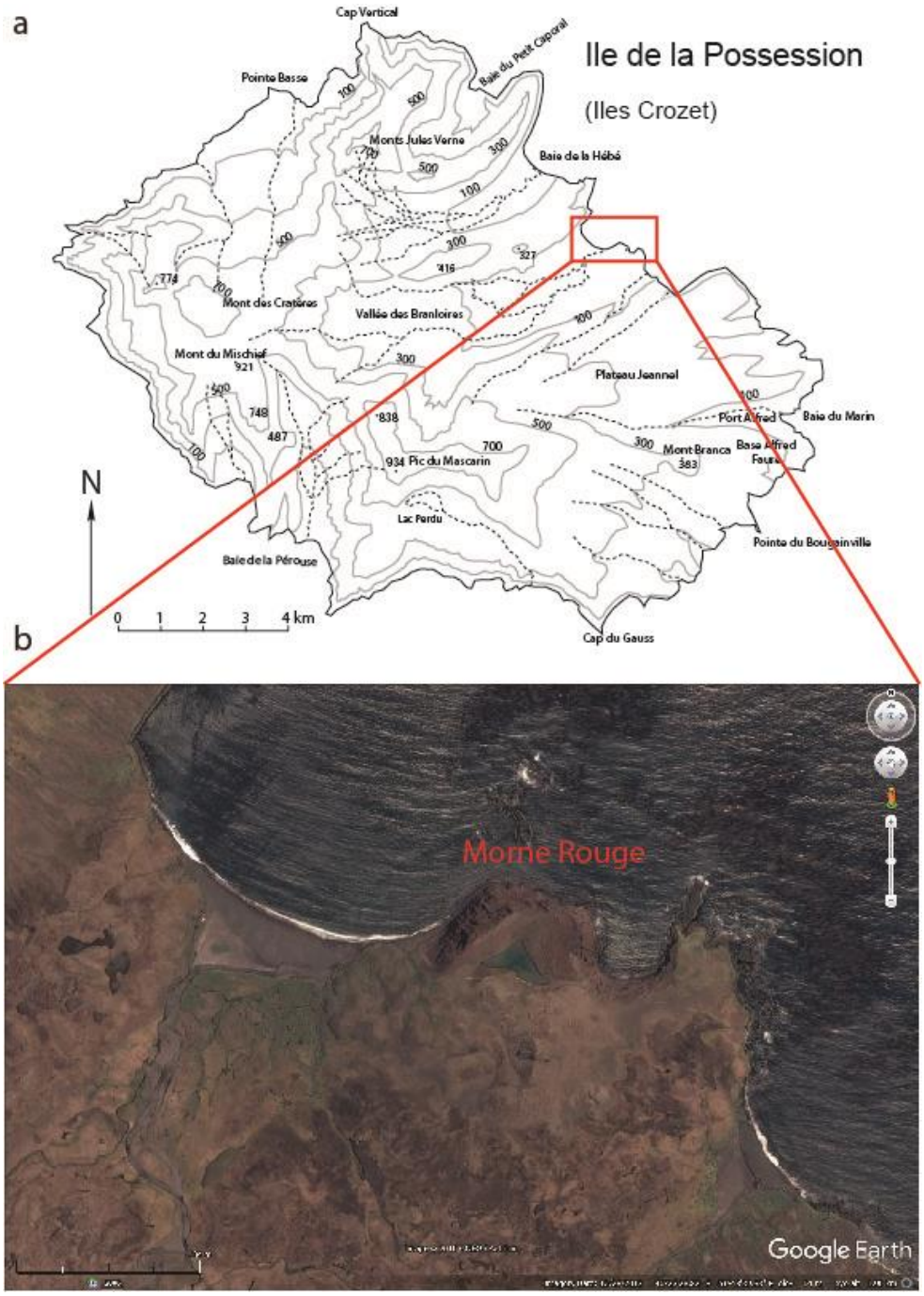

Figure S4: Ile de la Possession and location of the Morne Rouge. a, map of Ile de la Possession with the location of **b**, the Morne Rouge volcano with the lake showing the beach with black sands to the west of the crater (image taken from Google Earth 7.1.8.3036 (1/7/2017), 46°23'26"S – 51°48'47"E, http://www.earth.google.com).

Morne Rouge peat sequence XRF core-scanning

Part of the core (185-344 cm), covering the period of the Homeric minimum, was XRF- core-scanned. After cleaning and preparation of the archive-halve core surface and covering with SPEXCerti Ultralene® foil, the core was measured with the Avaatech instrument at NIOZ (Texel, the Netherlands) at both 10kV (500µA) and 30kV (150µA) covering the major elements Al, Si, P, S, Cl, K, Ca, Sc, Ti, V, Cr, Mn, Fe, Co, Ni, Cu, Zn, Ga, Ge, As, Se, Br, Rb, Sr, Y, Zr, Nb, Mo, Tc, Ru, Rh, Pd, Ag, Cd, In, Sn, Sb, Te, I, Cs, Ba, Hf, Ta, W, Re, Os, Ir, Pt, Au, Hg, Tl, Pb. at 10 kV and 500 µA and a second time at 30 kV and 150µA. A step size of 5 mm and a dwell time of 50 sec were used during scanning. The elemental data were normalised to the incoherent + coherent (inc + coh) scattering (Davies et al., 2015).

PCA was applied on the XRF data. Magnetic susceptibility (MS) and inc/coh (reflecting organic matter, see Davies et al.,2015) were incorporated in the data set. Data were standardized prior to analysis using the equation $z = (x - \mu)/\sigma$ in which μ is the mean and σ the standard deviation. PCA was performed using the PAST program (Hammer et al., 2001).

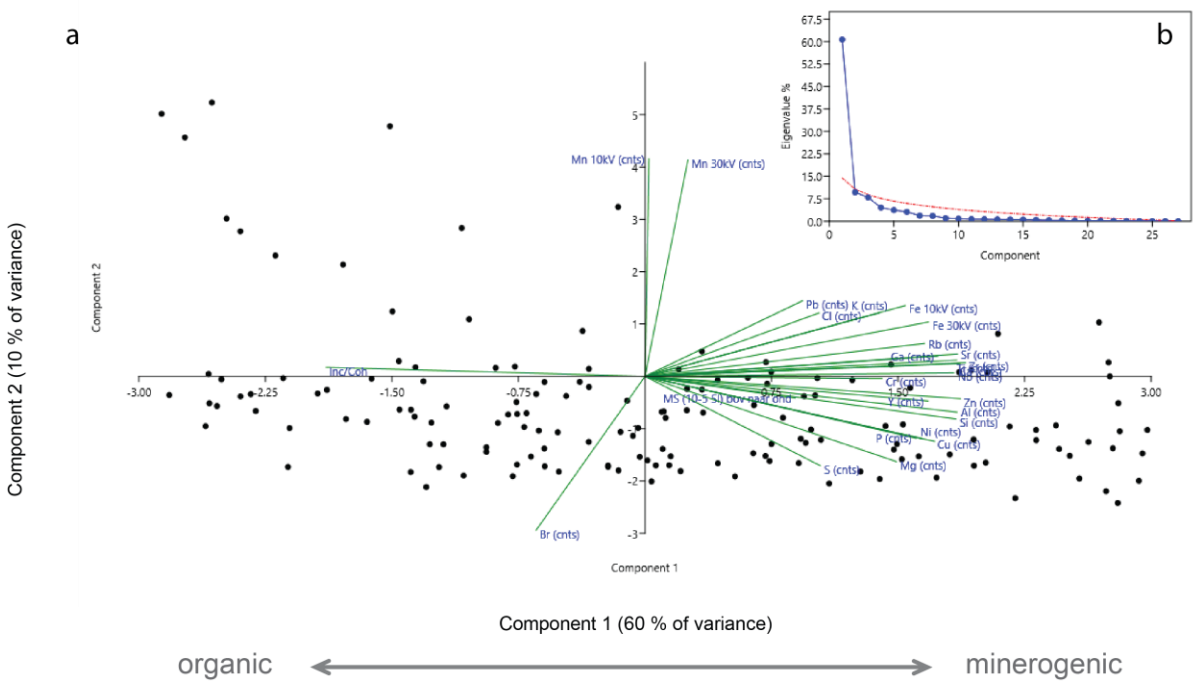

Figure S5: a, Scatter plot of first and second axes of a PCA on the Morne Rouge XRF core-scanning data **b**, scree plot with plotted eigenvalues of the principal components. Values under the Broken Stick random model curve (red curve) can be regarded as insignificant.

Reanalysis and modelling

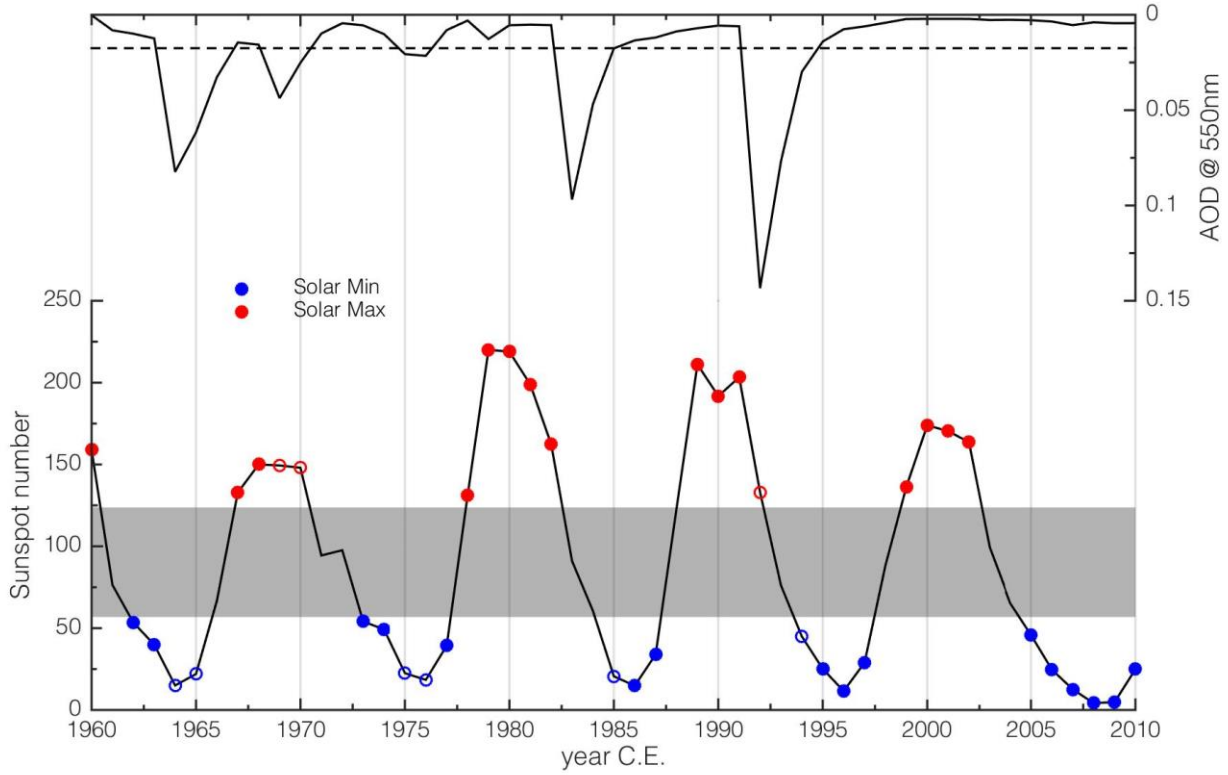

Figure S6: Definition of solar maximum and minimum years for the Reanalysis data. Top: 550nm aerosol optical depth (Sato et al., 1993) as a proxy for volcanic eruptions (solid black line) and the threshold used to identify years of volcanic forcing (dashed black line). Bottom: Annual International Sunspot Number (black line) (Clette et al., 2014). The grey patch indicates the threshold above (below) which years have been identified as solar maximum (minimum) years. Solar maximum years are shown as red circles, minimum years as blue circles. Open circles indicate where years have been excluded due to strong volcanic forcing (see top panel). The anomalies shown in Fig. 3 (Reanalysis panels), hence, represent differences between the December-February means of years marked with blue and red filled circles.

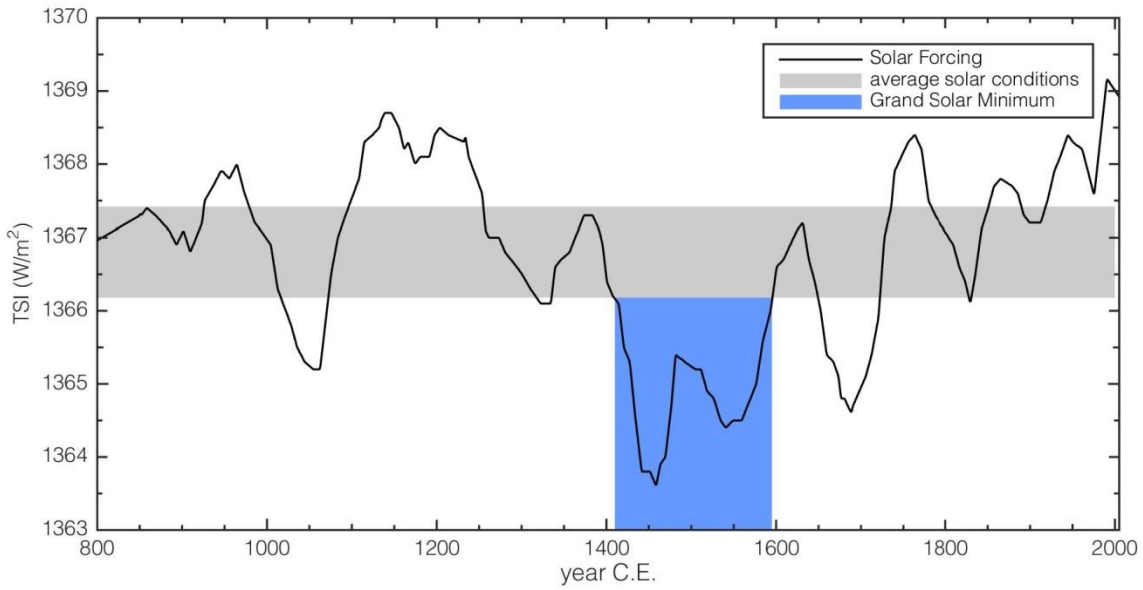

Figure S7: Definition of years covering the extent of the grand solar minimum in the climate model run. The black line shows the solar forcing applied in the model experiment (Bard et al., 2000). All other forcings were held constant. The grey patch encompasses the years used to define the climatology, i.e., 'normal' solar forcing. The blue patch highlights the grand solar minimum between ~1400 and 1600 C.E. used as an analogue to the Homeric grand solar minimum around 2,800 years ago. The Solar anomalies shown in Fig. 3 (model panels) refer to differences between the mean of years inside the blue and grey patch.

References

Bard, E., Raisbeck, G., Yiou, F., and Jouzel, J.: Solar irradiance during the last 1200 years based on cosmogenic nuclides, Tellus B, 52, 985-992, 2000.

Bronk Ramsey, C.: Deposition models for chronological records., Quaternary Science Reviews, 27, 42-60, 2008.

Bronk Ramsey, C.: Bayesian analysis of radiocarbon dates, Radiocarbon, 51, 337-360, 2009.

Clette, F., Svalgaard, L., Vaquero, J. M., and Cliver, E. W.: Revisiting the Sunspot Number, Space Science Reviews, 186, 35-103, 2014.

Compo, G. P., Whitaker, J. S., Sardeshmukh, P. D., Matsui, N., Allan, R. J., Yin, X., Gleason, B. E., Vose, R. S., Rutledge, G., Bessemoulin, P., Brönnimann, S., Brunet, M., Crouthamel, R. I., Grant, A. N., Groisman, P. Y., Jones, P. D., Kruk, M. C., Kruger, A. C., Marshall, G. J., Maugeri, M., Mok, H. Y., Nordli, Ø., Ross, T. F., Trigo, R. M., Wang, X. L., Woodruff, S. D., and Worley, S. J.: The Twentieth Century Reanalysis Project, Quarterly Journal of the Royal Meteorological Society, 137, 1-28, 2011.

Davies, S. J., Lamb, H. F., and Roberts, S. J.: Micro-XRF Core Scanning in Palaeolimnology: Recent Developments. In: Micor-XRF Studies of Sediment Cores, Croudace, I. W. and Rothwell, R. G. (Eds.), Developments in Palaeoenvironmental Rresearch, Springer Science+Business Media Dordrecht, 2015.

Hammer, Ø., Harper, D. A. T., and Ryan, P. D.: PAST: Paleontological statistics software package for education and data analysis, Palaeontol. Electron., 4, 9, 2001.

Hogg, A. G., Hua, Q., Blackwell, P. G., Niu, M., Buck, C. E., Guilderson, T. P., Heaton, T. J., Palmer, J. G., Reimer, P. J., Reimer, R. W., Turney, C. S. M., and Zimmerman, S. R. H.: SHCal13 Southern Hemisphere Calibration, 0–50,000 Years cal BP, Radiocarbon, 55, 1889-1903, 2013.

Hogg, A. G., Heaton, T. J., Hua, Q., Palmer, J. G., Turney, C. S. M., Southon, J., Bayliss, A., Blackwell, P. G., Boswijk, G., Bronk Ramsey, C., Pearson, C., Petchey, F., Reimer, P., Reimer, R., and Wacker, L.: SHCal20 Southern Hemisphere Calibration, 0–55,000 Years cal BP, Radiocarbon, 62, 759-778, 2020.

Mauquoy, D., Van Geel, B., Blaauw, M., and Van der Plicht, J.: Evidence from northwest European bogs show 'Little Ice Age' climatic changes driven by variations in solar activity., The Holocene, 12, 1-6, 2002.

Mellström, A., Van der Putten, N., Muscheler, R., De Jong, R., and Björck, S.: A shift towards wetter and windier conditions in southern Sweden around the prominent solar minimum 2750 cal a BP, Journal of Quaternary Science, 30, 235-244, 2015.

Pearson, G. W.: Precise Calendrical Dating of Known Growth-Period Samples Using a 'Curve Fitting' Technique, Radiocarbon, 28, 292-299, 1986.

Reimer, P. J., Bard, E., Bayliss, A., Beck, J. W., Blackwell, P. G., Bronk Ramsey, C., Buck, C. E., Cheng, H., Edwards, R. L., Friedrich, M., Grootes, P. M., Guilderson, T. P., Haflidason, H., Hajdas, I., Hatté, C., Heaton, T. J., Hoffmann, D. L., Hogg, A. G., Hughen, K. A., Kaiser, K. F., Kromer, B., Manning, S. W., Niu, M., Reimer, R. W., Richards, D. A., Scott, E. M., Southon, J. R., Staff, R. A., Turney, C. S. M., and van der Plicht, J.: IntCal13 and Marine13 Radiocarbon Age Calibration Curves 0–50,000 Years cal BP, Radiocarbon, 55, 1869-1887, 2013.

Sato, M., Hansen, J. E., McCormick, M. P., and Pollack, J. B.: Stratospheric aerosol optical depths, 1850–1990, Journal of Geophysical Research: Atmospheres, 98, 22987-22994, 1993.

Van der Putten, N., Hébrard, J.-P., Verbruggen, C., Van de Vijver, B., Disnar, J.-R., Spassov, S., Keravis, D., de Beaulieu, J.-L., De Dapper, M., Hus, J., Thouveny, N., and Frenot, Y.: An integrated palaeoenvironmental investigation of a 6200 year old peat sequence from Île de la Possession, Îles Crozet, sub-Antarctica., Palaeogeography, Palaeoclimatology, Palaeoecology, 270, 179-195, 2008.

van Geel, B. and Mook, W. G.: High-resolution 14C-dating of organic deposits using natural atmospheric 14C variations., Radiocarbon, 31, 151-155, 1989.